NANO LETTERS
Cite This: Nano Lett. 2019, 19, 8125−8131
Letter
pubs.acs.org/NanoLett

Terahertz-Driven Stark Spectroscopy of CdSe and CdSe−CdS Core−Shell Quantum Dots

Brandt C. Pein,*[,†] Chee Kong Lee,[†] Liang Shi,[†] JiaoJian Shi,[†] Wendi Chang,[†] Harold Y. Hwang,[‡] Jennifer Scherer,[†] Igor Coropceanu,[†] Xiaoguang Zhao,[§] Xin Zhang,[§] Vladimir Bulović,[†] Moungi G. Bawendi,[†] Adam P. Willard,[†] and Keith A. Nelson[†]

[†]Department of Chemistry and Department of Electrical Engineering and Computer Science, Massachusetts Institute of Technology, Cambridge, Massachusetts 02139 United States

[‡]Lincoln Laboratory, Massachusetts Institute of Technology, Lexington, Massachusetts 02420 United States

[§]Department of Mechanical Engineering, Boston University, Boston, Massachusetts 02215 United States

Supporting Information

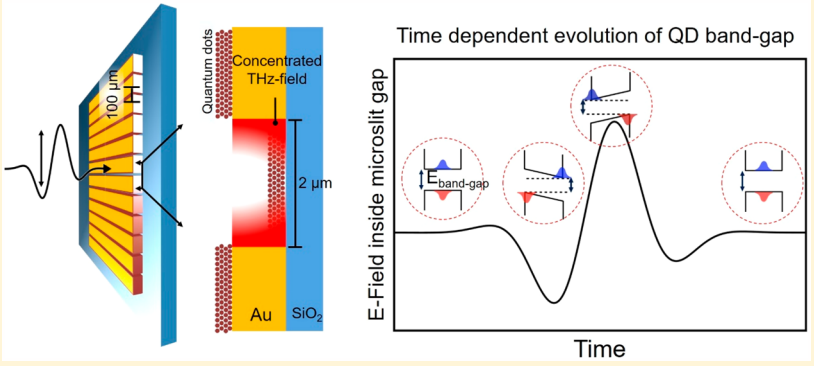

ABSTRACT: The effects of large external fields on semiconductor nanostructures could reveal much about field-induced shifting of electronic states and their dynamical responses and could enable electro-optic device applications that require large and rapid changes in optical properties. Studies of quasi-dc electric field modulation of quantum dot (QD) properties have been limited by electrostatic breakdown processes observed under high externally applied field levels. To circumvent this, here we apply ultrafast terahertz (THz) electric fields with switching times on the order of 1 ps. We show that a pulsed THz electric field, enhanced by a microslit field enhancement structure (FES), can strongly manipulate the optical absorption properties of a thin film of CdSe and CdSe−CdS core−shell QDs on the subpicosecond time scale with spectral shifts that span the visible to near-IR range. Numerical simulations using a semiempirical tight binding model show that the band gap of the QD film can be shifted by as much a 79 meV during these time scales. The results allow a basic understanding of the field-induced shifting of electronic levels and suggest electro-optic device applications.

KEYWORDS: *Terahertz, quantum dots, Stark effect, microslits*

The energies and momenta of electron and hole states in quantum dots (QDs) can be controlled by the application of alternating current (ac) and direct current (dc) electric fields via the quantum-confined Stark effect (QCSE).[1−5] Electronic control of QD electron and hole states, and by proxy the resulting refractive index, presents a useful path toward small and fast electro-optic devices.[6] For example, Hoffmann et al. have demonstrated that terahertz (THz) frequency signals can be encoded onto optical carrier light sources, via the QCSE, and achieve data transfer rates of at least 0.5 Tbit/s.[7] The extent that an ac electric field can manipulate quantum states by increasing the electric field strength is a potentially useful facet for device development; however, such large field control has its limits as the useful optical properties resulting from quantum confinement are destroyed from processes like dielectric breakdown or field emission of charge carriers. Here we explore the effects of large electric fields, in the MV/cm range, using ultrafast terahertz pulses coupled into a THz-frequency field enhancement structure (FES) spin coated with QDs. THz-frequency FESs are a common artifice for enhancing the electric and magnetic fields of THz pulses.[8−12] In addition, they are effective for applying large fields to QDs as their low duty cycle avoids dielectric breakdown.

We have previously demonstrated that large fields can reduce the bandgap of CdSe−CdS core−shell QDs by >0.5 e,

Received: August 14, 2019
Revised: October 2, 2019
Published: October 22, 2019

DOI: 10.1021/acs.nanolett.9b03342
Nano Lett. 2019, 19, 8125−8131

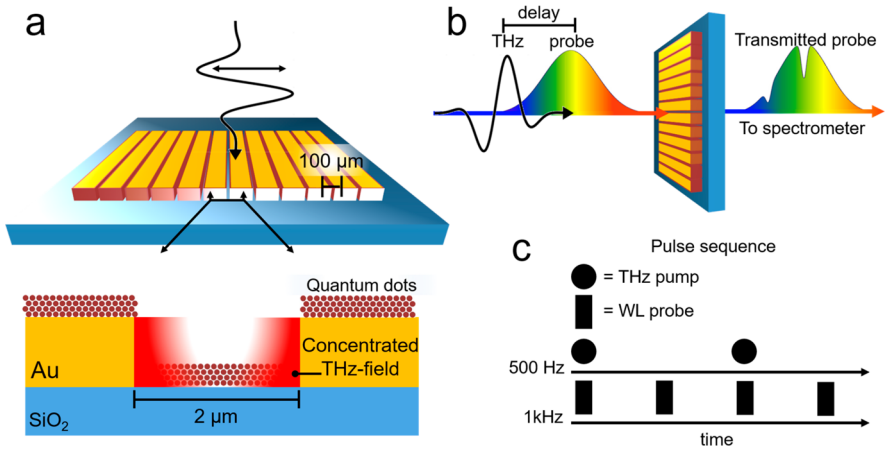

Figure 1. THz field-enhancing microslits and THz pump white light probe spectroscopy. (a) The microslits consist of 98 μm wide gold bars with 2 μm insulating gaps in between the bars. The microslits concentrate the THz electric field (polarized perpendicular to the bars) at each of the gaps. QDs deposited in those regions experience the enhanced THz electric field. (b) THz pump and white light probe pulses are focused onto the microslit array. The probe pulses are focused into a single gap whereas the pump pulses encompass multiple gaps. The pump and probe pulses are delayed relative to each other using a delay stage. The transmitted probe light is sent to the spectrometer. (c) The THz pump and white light probe pulses have repetition rates of 500 Hz and 1 kHz, respectively. This pulse sequence allows us to compare the zero-field and THz-modulated absorption spectra of the QD layer.

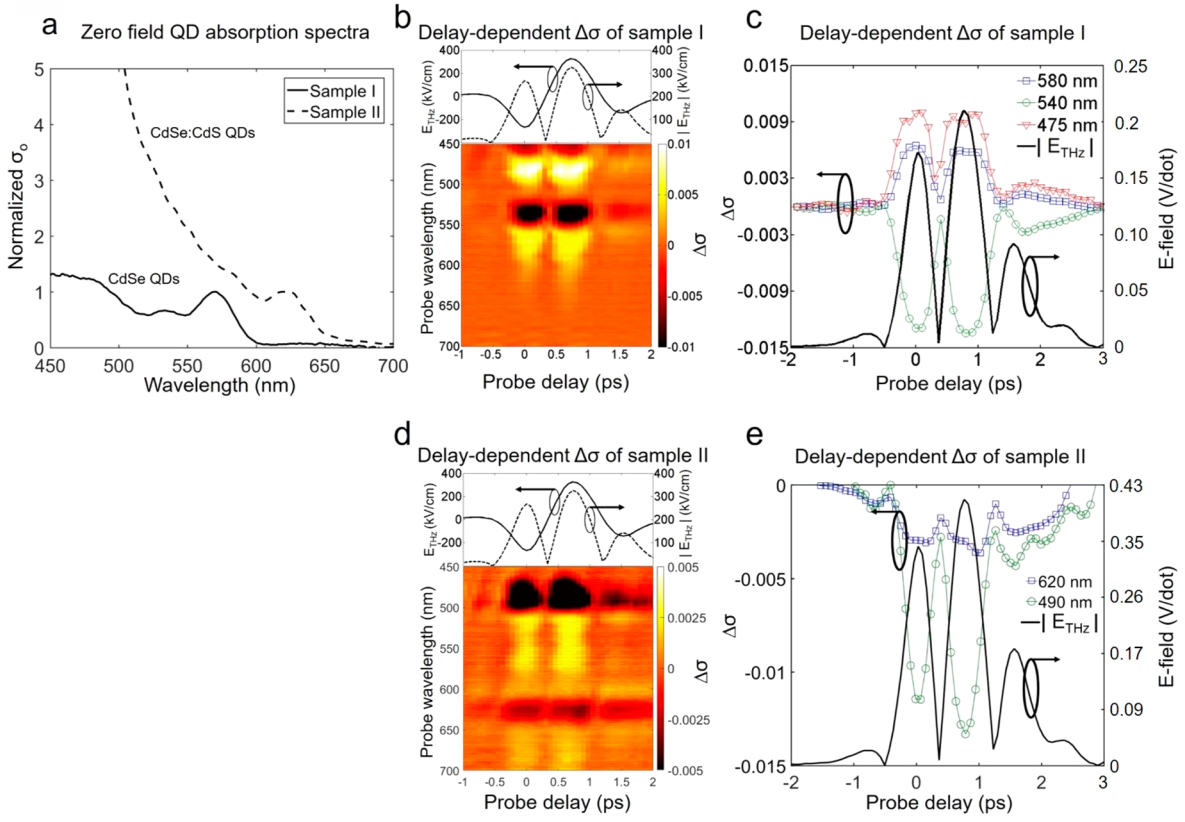

Figure 2. Zero-field absorption spectra and time-dependent absorption spectral changes. (a) The zero-field absorption spectra of both samples. Absorption peaks corresponding to optical transitions from the highest energy hole states to the lowest energy electron states are found at 570 and 620 nm for samples I and II, respectively. (b,d) The electric field and absolute value of the electric field of the THz pump pulses (top) have three distinct lobes. The arrival time of the first lobe at the sample is arbitrarily assigned as time $t = 0$. The electric field shifts the QD electronic states of Samples I and II which reduces and increases the absorption cross-section at different wavelengths (bottom). (c,e) Three and two wavelengths from the delay-dependent $\Delta\sigma$ spectrum of Samples I and II, respectively, are plotted along with the absolute value of the THz electric field (in V/dot). In both samples the changes in the absorption spectra track the THz electric field.

and excite electrons leading to visible light luminescence.[13] These observations were indicative of significant electronic state modulation, however we were probing the lowest energy optical transitions composed of the lowest energy conduction band or highest energy valence band states and had no information about the rest of the state manifold. In the work presented here, using transient white-light absorption spectroscopy, we observed changes in the visible to near-IR

DOI: 10.1021/acs.nanolett.9b03342
Nano Lett. 2019, 19, 8125−8131

absorption spectra of thin films of CdSe and CdSe−CdS QDs that were subjected to multi-MV/cm THz electric fields. Our goal is to introduce a more complete measurement of the field modulated optical transitions. We demonstrate that large THz fields induce absorption spectrum shifts across much of the visible spectrum and into the near-IR on time scales similar to those of the applied THz field. We explain the results in terms of the QCSE based on numerical simulations using a tight-binding model.[14]

We used a simple FES design, a microslit array, consisting of parallel gold lines with 98 μm widths separated by 2 μm capacitive gaps on a SiO_2 substrate (Figure 1a). The arrays were coated with 30−40 nm thick layers of QDs that were deposited by spin coating solutions of QDs suspended in hexane. Two QD samples were used: 4 nm diameter CdSe QDs (Sample I) and 8 nm diameter CdSe−CdS core−shell QDs that had a 4 nm diameter core and a 2 nm thick shell (Sample II) (see Supporting Information for details on QD synthesis). We chose these particular samples because the cores do not luminesce at these fields strengths whereas the core−shell QDs do, primarily due to their larger diameter leading to a larger voltage drop across the QD. In our previous study, THz-induced luminescence lifetime measurements indicated the presence of charged QD states lasting ∼1 ns which would potentially hinder any THz frequency device applications. As we will show, charged QD states do not appear to contribute to the THz modulation and the resulting absorption spectrum changes.

THz pulses with a 325 kV/cm peak electric-field polarized perpendicular to the gold lines were focused onto the microslit arrays. To measure time-dependent THz-modulated absorption spectra, white-light probe pulses were generated by 100 fs, 810 nm pulses in a sapphire window, focused into a single microslit gap, and variably delayed relative to the THz excitation pulse arrival time (Figure 1b). The white-light probe had a usable spectral bandwidth spanning 450−700 nm. The transmitted probe spectra were collected at a 1 kHz repetition rate and the THz excitation pulses were modulated with an optical chopper to reduce their repetition rate to 500 Hz (Figure 1c). As such, the probe spectra were collected in pairs, one with the THz excitation pulse, measuring

$$I_{\mathrm{THz+probe}}(\lambda) \propto CI_{\mathrm{o}}(\lambda)e^{-\sigma_{\mathrm{Stark}}(\lambda)} \tag{1}$$

and the other without the THz pulse, measuring

$$I_{\mathrm{probe}}(\lambda) \propto CI_{\mathrm{o}}(\lambda)e^{-\sigma_{\mathrm{o}}(\lambda)} \tag{2}$$

where $I_0(\lambda)$ is the incident white-light probe intensity, $\sigma_{\mathrm{Stark}}(\lambda)$ is the Stark-shifted absorption cross section, $\sigma_{\mathrm{o}}(\lambda)$ is the zero-field absorption cross section, and C depends on the sample concentration and optical path length which are constant in both cases. Figure 2a shows the zero-field absorption spectra, $\sigma_{\mathrm{o}}(\lambda)$, of both samples which show distinguishable peaks at 570 and 620 nm for samples I and II, respectively, corresponding to optical transitions from the highest energy hole states to the lowest energy electron states. The change in the absorption spectrum $\Delta\sigma(\lambda)$ is computed as

$$\Delta\sigma(\lambda) = -\ln\left(\frac{I_{\mathrm{THz+probe}}(\lambda)}{I_{\mathrm{probe}}(\lambda)}\right) = \sigma_{\mathrm{Stark}}(\lambda) - \sigma_{\mathrm{o}}(\lambda) \tag{3}$$

Figure 2b,d shows the time-dependent $\Delta\sigma$ spectrum of samples I and II, respectively, and Figure 2c,e shows time-dependent traces for a few selected wavelengths along with the absolute value of the incident THz electric field. It is apparent that the spectral changes follow the dynamics of the THz field, showing that subpicosecond spectral modulation and electro-optic effects are achievable. Although the absorption spectrum tracks the absolute value of the THz electric field, it is important to note that we do not take this to necessarily mean that the polarity of the THz field has no effect on the absorption spectrum changes. (See Supporting Information for details on THz/white light generation and time-dependent $\Delta\sigma$ spectrum data workup.)

The absorption spectrum modulation could originate from the enhanced THz field or from charges,[1,7,13,15] more specifically charged QDs, generated by the THz field. To understand the origin of the changes in the absorption spectrum it is important to isolate these two sources. In our previous work,[13] we found that QDs could be driven to luminescence via charge separation between neighboring QDs when the voltage drop between QDs multiplied by the fundamental charge unit was equal to or greater than the band gap energy. For samples I and II, this is >2 V/dot. Although parts of a microslit gap experience fields >2 V/dot, QDs found in these regions make up ∼0.5% of the total probed volume (see Supporting Information for details) so the probe signals are dominated by QDs experiencing THz fields below the threshold required for charge separation. The time-dependent $\Delta\sigma$ spectra track the rise and fall of the THz electric field and have no measurable contributions from longer-lived QD states. In contrast, our previous work revealed that the above-threshold THz-induced luminescence had a shorter lifetime (∼1 ns) compared to the optically induced luminescence (15 ns), indicating that charged states (and presumably any absorption spectral shifts resulting from them) persisted for longer than the 1 ps time scale of the THz field. We therefore believe the observed $\Delta\sigma$ spectra are generated entirely by the THz electric field effects on QD electronic energy levels without any significant contribution from charged states.

The time-dependent absorption spectrum provides dynamical information about the THz modulated states, though it is admittedly difficult to extract the field dependence of the state energies from the absorption spectrum shifts. This is mainly due to the line widths of the optical transitions that make up the QD absorption spectra and the large number thereof that are all simultaneously shifting under the applied THz field. To understand the underlying changes in the QD electronic states and the resulting modulated absorption spectra, we performed simulations of both types of QDs found in samples I and II subjected to an external dc electric field. The solutions for electron and hole states are found using a full-atomistic, semiempirical tight binding model[14] with previously established material parameters.[16,17] The crystals are modeled as defect-free and unstrained spheres with open boundary condition and a lattice constant of 5.82 Å. The electric field is introduced into the tight-binding Hamiltonian by shifting the on-site energies by the potential

$$V(\vec{r}) = e\vec{F}\cdot\vec{r} \tag{4}$$

extracted at each atomic position $\vec{r}_i$, where e is the electron charge and $\vec{F}$ is the applied electric field. The oscillator strengths are proportional to the absorption cross sections σ of transitions between electron and hole states and to the optical matrix elements P which are calculated by

DOI: 10.1021/acs.nanolett.9b03342
Nano Lett. 2019, 19, 8125−8131

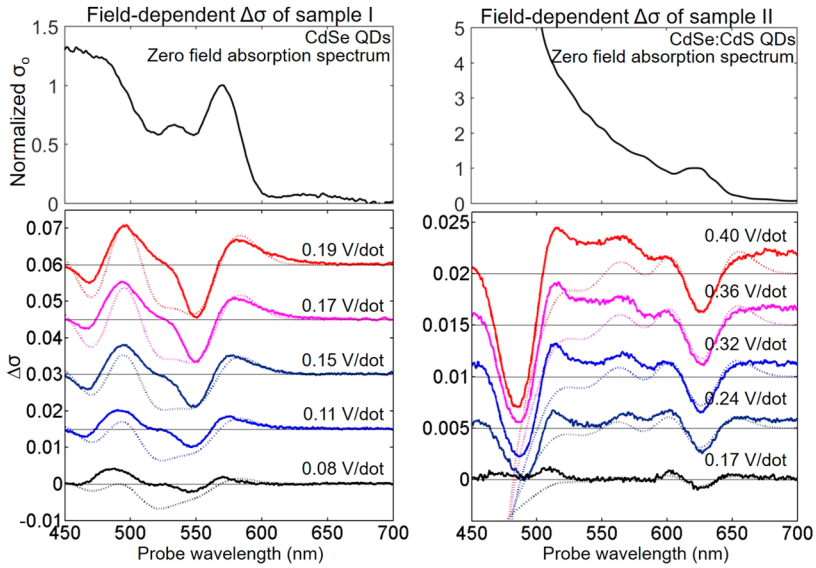

Figure 3. Field-dependent $\Delta\sigma$ spectra of samples I and II compared with simulations. The THz-pump white light-probe delay was fixed at 1 ps corresponding to the second THz field lobe which is the strongest of the three. A pair of wire-grid polarizers was used to attenuate the field strength of the THz pulses while measuring the $\Delta\sigma$ spectrum of both samples (solid lines). Each simulated optical transition was assigned a Gaussian line shape with a height proportional to its oscillator strength. The fwhm of all the Gaussian features was assumed to be the same and was assigned a value that best fit the experimental data. The simulated $\Delta\sigma$ spectra (dashed lines) capture many of the qualitative features seen in the experimental data, through there are clear quantitative and some qualitative discrepancies.

$$P = |\langle\psi_e|\vec{p}\,|\psi_h\rangle|^2 \tag{5}$$

where $|\psi_e\rangle$ ($|\psi_h\rangle$) is the electron (hole) wave function and $\vec{p}$ is the momentum operator. To determine the electric time-dependent field strength used in the tight-binding simulations (F in eq 4) the field time-dependent enhancement within a microslit gap was simulated using CST microwave studio.[18] Nearest to the gold surfaces, making up the inner vertical walls of a microslit gap, enhancement factors can reach as high as 140. Considering a uniform QD layer over the surface of a microslit gap, only ~0.5% of the QDs reside in these regions with large enhancement whereas the rest lie on the surface of the SiO_2 substrate (inside the microslit gap) where the average field enhancement is 16.5 (see Supporting Information for details).

At the microslit gaps, the electric-field experienced by individual QDs is $\vec{F}(V/\text{dot}) = \vec{F}_{THz}\beta/\varepsilon_{QD}$ where F_{THz} is the incident THz electric field, β is the enhancement factor, and ε_{QD}, the dielectric constant of an individual quantum dot, is 11.6 for sample I and 10.9 for sample II, both determined using the Maxwell-Garnet effective medium approximation

$$\varepsilon_{QD} = \varepsilon_{CdS} + 3\varepsilon_{CdS}\left(\frac{R_{core}}{R_{shell}}\right)^3\left(\frac{\varepsilon_{CdSe} - \varepsilon_{CdS}}{\varepsilon_{CdSe} + 2\varepsilon_{CdS} - \left(\frac{R_{core}}{R_{shell}}\right)^3(\varepsilon_{CdSe} - \varepsilon_{CdS})}\right) \tag{6}$$

where R_{core} (R_{shell}) is the radius of the core (shell), ε_{CdS} is 10.8, and ε_{CdSe} is 11.6.[19] The QDs are covered in organic ligands which will reduce the electric field they experience. To account for this, we approximate the QDs within the microslit gap as a series of capacitors as suggested by Bozyigit et al.[3] In their treatment,[3] the dielectric constant of the film is

$$\varepsilon_{film} = \frac{1}{\frac{f_{QD}}{\varepsilon_{QD}} + \frac{(1-f_{QD})}{\varepsilon_{org}}} \tag{7}$$

where f_{QD} is the fill factor of the QD inclusions of the film, ε_{QD} is the dielectric constant of the QDs, and ε_{org} is the dielectric constant of the organic ligands which we assume is 2.2 based on similar types of samples.[3] From this we can compute the electric field experienced by the film. To get the field experienced by the QDs themselves, the above equation is divided by ε_{QD} to give

$$\frac{F_{QD}}{F_{film}} = \frac{\varepsilon_{film}}{\varepsilon_{QD}} = \frac{\varepsilon_{org}}{f_{QD}\varepsilon_{org} + (1-f_{QD})\varepsilon_{QD}} \tag{8}$$

From SEM images of the QDs (see Supporting Information), we estimate a fill factor of 0.5 for sample I and 0.75 for sample II. Furthermore, it has been previously shown that optical excitation of QDs can change the dielectric constant. Here, we assume that the white light probe is weak enough such that it does not appreciably change the dielectric constant of the QD film.

Figure 3 shows the experimental and simulated field-dependent $\Delta\sigma$ spectra of both samples. Note that the ranges of field strength are not the same for both samples since the diameters of the two types of QDs are different. The experimental $\Delta\sigma$ spectra were extracted by varying the incident THz field strength with a pair of wire grid polarizers and at each field level, recording the modulated absorption spectra at a probe delays corresponding to the maximum THz field lobe at ~1 ps. To plot the simulated $\Delta\sigma$ spectra, each of the computed optical transitions was assigned a Gaussian line shape with height proportional to the simulated oscillator strength P. The widths of the lines were assumed to be equal, and the value that best fit the spectra was used. We assign no physical meaning to a Gaussian line shape which was chosen for convenience in the fitting to our experimental data.

The simulated $\Delta\sigma$ spectra capture most of the features of the experimental data though there are some obvious discrepancies particularly in the case of sample II. In sample II, at wavelengths <500 nm the simulated data predict a far more

DOI: 10.1021/acs.nanolett.9b03342
Nano Lett. 2019, 19, 8125−8131

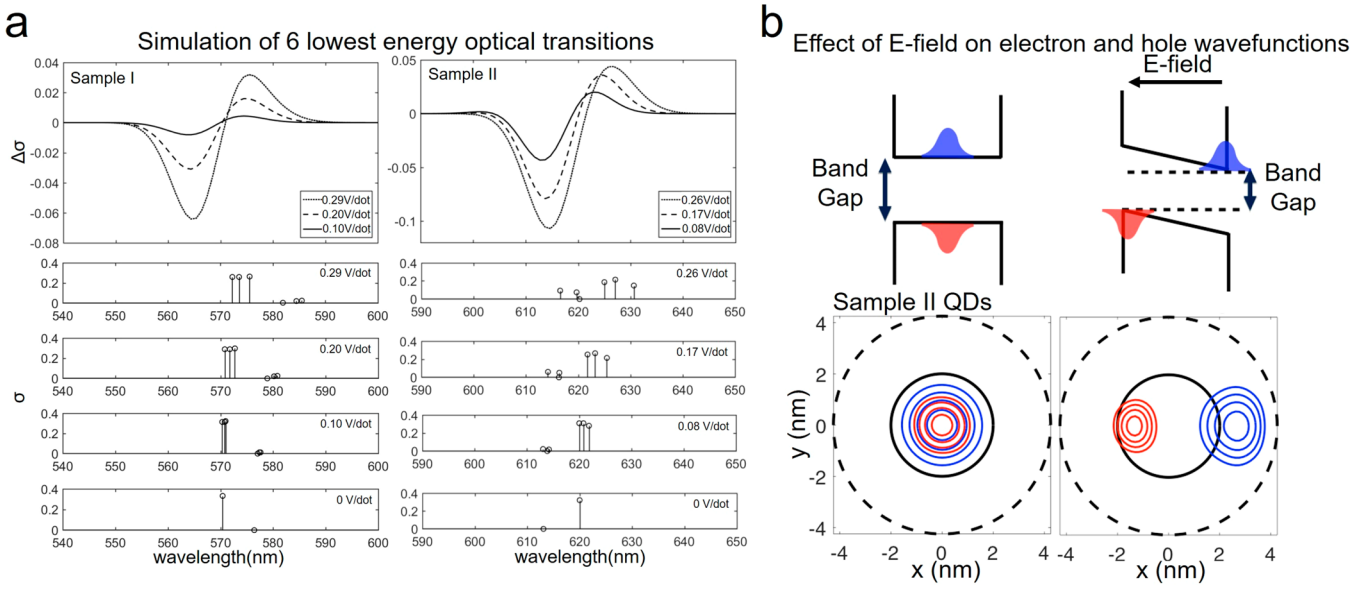

Figure 4. Simulation of the six lowest-energy optical transitions and effects of electric field on electron/hole wave functions. (a) Under zero electric field, the six lowest-energy optical transitions consist of two sets of 3-fold degenerate transitions due to the 3-fold degeneracy of the hole p-orbital states. In both samples, one of the sets of 3-fold degenerate transitions is forbidden due a phase mismatch between the electron and hole wave functions. The other sets have large oscillator strengths which give rise to the experimental zero-field absorption spectra at 570 and 620 nm for samples I and II, respectively. Under an increasing external electric field, the 3-fold degeneracies are lifted, the oscillator strength of each transition is changed, and the transition energies are red-shifted. (b) The redshifting of transitions is explained by the tilting of the valence and conduction bands (top). The reduction in oscillator strength is explained by reduced overlap electron and hole wave functions (bottom) as positive and negative charges are moved to opposite sides of the QD. Conversely, the increase in oscillator strength is explained by a removal of the electron and hole phase mismatch by the electric field.

drastic reduction in the absorption cross section. We believe this is from inaccurate simulation of optical transitions at these wavelengths due to the limited number of electron and hole wave functions used in the simulations. This discrepancy also applies to sample I at shorter wavelengths than sample II. At wavelengths >650 nm, the simulated $\Delta\sigma$ spectrum of sample II is drastically underestimated compared to experiment. Because the usable spectral bandwidth of the white light probe encompasses 450−700 nm, it is impossible tell how far the increase in absorption extends into the near-IR. In our previous work,[13] we demonstrated that the increase can extend to >850 nm for the same QDs found in sample II.

From our simulations, we can gain some insight into the changes of the underlying QD electronic structure under the influence of the THz-induced QCSE. Our simulations yield a large set of electronic transitions that span a wide range of transition energies. Here, we focus on the six lowest energy transitions, which dominate the spectral features that are illustrated in Figure 3. The positive $\Delta\sigma$ for wavelengths longer than 570 and 620 nm for samples I and II, respectively, is largely determined by these six transitions from the three highest energy hole states to the two lowest energy electron states. In the absence of the electric field, three of the transitions are from 3-fold degenerate hole states, due to the 3-fold degeneracy of the p-orbitals, which are strongly coupled to the second lowest electronic state in sample I and the lowest electronic state in sample II. These degenerate transitions are reflected by the large oscillator strength at 570 and 620 nm for samples I and II, respectively, under zero field (Figure 4a). As the field strength increases, the transitions are red-shifted due to the tilting of the energy bands and broadened due to the splitting of the 3-fold degenerate hole states which results in negative peaks at 570 and 620 nm for samples I and II, respectively, and positive peaks at longer wavelengths in the $\Delta\sigma$ spectra.

Because electrons and holes are oppositely charged, their corresponding wave functions spatially shift in opposite directions under the external electric field as illustrated in Figure 4b for a core−shell QD as in Sample II. Consequently wave function overlap between electron and hole is reduced, leading to decreased oscillator strength. On the other hand, in the absence of the THz electric field the wave function overlaps between the degenerate hole states and the lowest electron state in sample I and the second lowest electronic state in sample II are zero due to phase mismatch, resulting in zero oscillator strength for sample I at 576 nm and sample II at 613 nm. The phase mismatch is removed by the application of electric field, leading to an increase in oscillator strength.

Although we focus our discussion on the lowest energy optical transitions, it is still relevant to discuss the changes in the absorption spectrum at shorter wavelengths which is composed of higher energy electronic states. It is beyond this work to make generalized statements about how these states shift under an applied THz field other than they behave similar to their lower energy counterparts which has consequences for the magnitude of the absorption spectrum changes. In Figure 3, the $\Delta\sigma$ spectrum of sample II shows the largest absorption changes for wavelengths <500 nm. This is primarily due to the large number of optical transitions that make up absorption spectrum in this range which are all simultaneously shifting and changing their oscillator strength. In sample I, this is not the case because the bulk of the optical transitions in the sample are outside the visible probe bandwidth. From a device application standpoint, this is a potential relevant variable for increasing the THz-modulation of an optical signal.

DOI: 10.1021/acs.nanolett.9b03342
Nano Lett. 2019, 19, 8125−8131

The shifting of the conduction and valence bands under an externally applied electric field gives rise to the reduced bandgap as discussed above. Because of the spectral broadening observed in our experimental $\Delta\sigma$ spectra, be it from the simulated mechanisms discussed above or due to sample heterogeneity, it is impossible to give a reliable experimental value of the bandgap reduction. However, it is still worthwhile to discuss what our simulations predict. The simulated bandgap, being the lowest energy transition, as a function of the applied field strength is plotted in Figure 5 for both samples. Considering the polar and polarizable character of the lowest energy transition, the band gap energy E_{gap} can be described with the excited state dipole moment μ and polarizability α

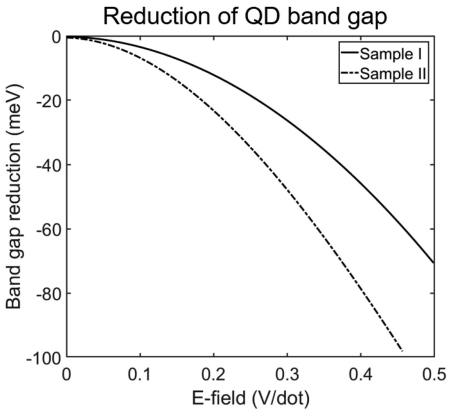

Figure 5. Simulation of QD band gap reduction. Simulation of the lowest energy transitions for both samples. The largest experimental field applied is 0.19 and 0.4 V/dot for samples I and II, respectively; these field strengths correspond to predicted band gap reductions of −12 and −79 meV for samples I and II, respectively.

$$E_{gap} = E_o + \mu F + \alpha F^2 \quad (9)$$

where F is the electric field projected onto μ and α and E_o is the zero-field band gap energy. Fitting eq 7 to the simulated band gap, the QDs in sample I have simulated μ and α values of 7.26 D and 1.33×10^4 (Å^3), respectively, whereas the QDs in sample II have values of 15.0 D and 3.48×10^4 (Å^3), respectively. The polarizability components are consistent with previous works utilizing THz fields to measure exciton polarizability in CdSe QDs.[20,21] The QDs in sample I have half the radius of QDs in sample II so the simulated dipole moments are also consistent with scaling approximations that one would predict, namely, $\mu \sim eR$ where R is the radius of the QD. Considering the strongest THz fields applied to the samples in our experiments and our simulations, we predict a band gap reduction of −12 and −79 meV for samples I and II, respectively. It should be noted that these predicted band gap reductions apply to the majority of the QDs found at the microslit gaps. As discussed earlier, ∼0.5% of the QD film lies near the gold surfaces of the gaps where significantly higher field enhancement is found and the THz electric field can be >10 times as strong compared to the middle of the gaps on the SiO_2 substrates. Note that in our previous work the enhanced THz field shifted the band gap of core−shell QDs by 0.55 eV based off photoluminescence measurements. In that work, we found that core−shell QDs with a band gap of 2.0 eV generated photoluminescence when 1.45 eV optical pulses were spatiotemporally overlapped with THz pulses within the microslit gaps. This indicated that a population of QDs, those experiencing the strongest field, had a band gap reduction of 0.55 eV and subsequently the absorbed the 1.45 eV photons and photoluminescence was observed. It must be stressed that this method was sensitive to QDs experiencing only the strongest enhanced THz field whereas the absorption measurements presented in this current work are indicative of the majority of the QDs within the slit gaps.

We have demonstrated that THz electric fields enhanced by a microslit FES can significantly change the electronic structure of QDs. The electron and hole states are red-shifted, leading to changes in the absorption spectrum spanning the entire visible spectrum and into the near IR and a reduction of the bandgap as large as −79 meV. The capability of modifying broadband optical properties of semiconducting materials using THz-frequency electric fields has potential applications for THz-frequency electro-optics or wireless communications in which THz-frequency information could potentially be encoded onto optical light sources.

■ ASSOCIATED CONTENT

Supporting Information

The Supporting Information is available free of charge on the ACS Publications website at DOI: 10.1021/acs.nanolett.9b03342.

Description of the experimental apparatus and generation of ultrafast terahertz pulses; details of time-dependent $\Delta\sigma$ spectrum data workup; details of quantum dot synthesis and characterization; microslit characterization including fabrication and electromagnetic simulations; details of quantum dot distribution within microslit gaps (PDF)

■ AUTHOR INFORMATION

Corresponding Author

*E-mail: bpein@mit.edu. Phone: 617-588-2128.

ORCID

Brandt C. Pein: 0000-0002-6145-1361
Igor Coropceanu: 0000-0001-8057-1134
Xin Zhang: 0000-0002-4413-5084
Moungi G. Bawendi: 0000-0003-2220-4365
Adam P. Willard: 0000-0002-0934-4737

Author Contributions

B.C.P. and K.A.N. conceived the study. I.C. and J.S. synthesized and characterized the QDs used in the experiments. H.Y.H., X. Zhao, and X. Zhang fabricated the microslit field enhancement structures. H.Y.H. performed the electromagnetic simulations of the microslit field enhancement structures. C.K.L. and L.S. performed the quantum dot simulations and interpreted the results. B.C.P., J.J.S., and W.C. collected all spectroscopic data. B.C.P prepared the manuscript with the assistance of C.K.L. and K.A.N. All authors read and commented on the manuscript.

Notes

The authors declare no competing financial interest.

■ ACKNOWLEDGMENTS

W.C., V.B., J.S., I.C., M.B., and K.A.N. were supported as part of the Center for Excitonics, an Energy Frontier Research Center funded by the U.S. Department of Energy, Office of

DOI: 10.1021/acs.nanolett.9b03342
Nano Lett. 2019, 19, 8125−8131

Science, Office of Basic Energy Sciences under Award Number DE-C0001088. H.Y.H., B.C.P., and J.J.S. were supported by Office of Naval Research Grants N00014-13-1-0509 and N00014-16-1-2090. J.J.S. was also supported by U.S. Army Research Office through the Institute for Soldier Nanotechnologies under Cooperative Agreement Number W911NF-18-2-0048 and the Samsung Global Research Outreach program. Equipment for the project was provided by Office of Naval Research Grant N00014-15-1-2879. X. Zhao and X. Zhang acknowledge NSF Grant ECCS 1810252.

■ ABBREVIATIONS

QD, quantum dot; QCSE, quantum-confined Stark effect; THz, terahertz; FES, field-enhancement structure; CST, computer simulation technology

■ REFERENCES

(1) Empedocles, S. A. Quantum-Confined Stark Effect in Single CdSe Nanocrystallite Quantum Dots. *Science (Washington, DC, U. S.)* **1997**, *278* (5346), 2114−2117.
(2) Bennett, A. J.; Patel, R. B.; Skiba-Szymanska, J.; Nicoll, C. A.; Farrer, I.; Ritchie, D. A.; Shields, A. J. Giant Stark Effect in the Emission of Single Semiconductor Quantum Dots. *Appl. Phys. Lett.* **2010**, *97* (3), 031104.
(3) Bozyigit, D.; Yarema, O.; Wood, V. Origins of Low Quantum Efficiencies in Quantum Dot LEDs. *Adv. Funct. Mater.* **2013**, *23* (24), 3024−3029.
(4) Bozyigit, D.; Wood, V.; Shirasaki, Y.; Bulovic, V. Study of Field Driven Electroluminescence in Colloidal Quantum Dot Solids. *J. Appl. Phys.* **2012**, *111* (11), 113701.
(5) Wood, V.; Halpert, J. E.; Panzer, M. J.; Bawendi, M. G.; Bulović, V. Alternating Current Driven Electroluminescence from ZnSe/ZnS:Mn/ZnS Nanocrystals. *Nano Lett.* **2009**, *9* (6), 2367−2371.
(6) Faraon, A.; Majumdar, A.; Kim, H.; Petroff, P.; Vučković, J. Fast Electrical Control of a Quantum Dot Strongly Coupled to a Photonic-Crystal Cavity. *Phys. Rev. Lett.* **2010**, *104* (4), 047402.
(7) Hoffmann, M. C.; Monozon, B. S.; Livshits, D.; Rafailov, E. U.; Turchinovich, D. Terahertz Electro-Absorption Effect Enabling Femtosecond All-Optical Switching in Semiconductor Quantum Dots. *Appl. Phys. Lett.* **2010**, *97* (23), 231108.
(8) Liu, M.; Hwang, H. Y.; Tao, H.; Strikwerda, A. C.; Fan, K.; Keiser, G. R.; Sternbach, A. J.; West, K. G.; Kittiwatanakul, S.; Lu, J.; et al. Terahertz-Field-Induced Insulator-to-Metal Transition in Vanadium Dioxide Metamaterial. *Nature* **2012**, *487* (7407), 345−348.
(9) Fan, K.; Hwang, H. Y.; Liu, M.; Strikwerda, A. C.; Sternbach, A.; Zhang, J.; Zhao, X.; Zhang, X.; Nelson, K. A.; Averitt, R. D. Nonlinear Terahertz Metamaterials via Field-Enhanced Carrier Dynamics in GaAs. *Phys. Rev. Lett.* **2013**, *110* (21), 217404.
(10) Tarekegne, A. T.; Iwaszczuk, K.; Zalkovskij, M.; Strikwerda, A. C.; Jepsen, P. U. Impact Ionization in High Resistivity Silicon Induced by an Intense Terahertz Field Enhanced by an Antenna Array. *New J. Phys.* **2015**, *17* (4), 043002.
(11) Padilla, W. J.; Taylor, A. J.; Highstrete, C.; Lee, M.; Averitt, R. D. Dynamical Electric and Magnetic Metamaterial Response at Terahertz Frequencies. In *2006 Conference on Lasers and Electro-Optics and 2006 Quantum Electronics and Laser Science Conference*; IEEE, 2006; pp 1−2.
(12) Chen, H.-T.; Padilla, W. J.; Zide, J. M. O.; Gossard, A. C.; Taylor, A. J.; Averitt, R. D. Active Terahertz Metamaterial Devices. *Nature* **2006**, *444* (7119), 597−600.
(13) Pein, B. C.; Chang, W.; Hwang, H. Y.; Scherer, J.; Coropceanu, I.; Zhao, X.; Zhang, X.; Bulović, V.; Bawendi, M.; Nelson, K. A. Terahertz-Driven Luminescence and Colossal Stark Effect in CdSe-CdS Colloidal Quantum Dots. *Nano Lett.* **2017**, *17*, 5375.
(14) Luisier, M.; Schenk, A.; Fichtner, W.; Klimeck, G. Atomistic Simulation of Nanowires in the s p 3 d 5 s * Tight-Binding Formalism: From Boundary Conditions to Strain Calculations. *Phys. Rev. B: Condens. Matter Mater. Phys.* **2006**, *74* (20), 205323.
(15) Caruge, J. M.; Halpert, J. E.; Wood, V.; Bulović, V.; Bawendi, M. G. Colloidal Quantum-Dot Light-Emitting Diodes with Metal-Oxide Charge Transport Layers. *Nat. Photonics* **2008**, *2* (4), 247−250.
(16) Lippens, P. E.; Lannoo, M. Comparison between Calculated and Experimental Values of the Lowest Excited Electronic State of Small CdSe Crystallites. *Phys. Rev. B: Condens. Matter Mater. Phys.* **1990**, *41* (9), 6079−6081.
(17) Lippens, P. E.; Lannoo, M. Calculation of the Band Gap for Small CdS and ZnS Crystallites. *Phys. Rev. B: Condens. Matter Mater. Phys.* **1989**, *39* (15), 10935−10942.
(18) CST.com. www.cst.com/products/cstmws (Accessed Oct 2018).
(19) Palik, E. D. *Handbook of Optical Constants of Solids*; Academic Press, 1998.
(20) Wang, F.; Shan, J.; Islam, M. A.; Herman, I. P.; Bonn, M.; Heinz, T. F. Exciton Polarizability in Semiconductor Nanocrystals. *Nat. Mater.* **2006**, *5*, 861.
(21) Dakovski, G. L.; Lan, S.; Xia, C.; Shan, J. Terahertz Electric Polarizability of Excitons in PbSe and CdSe Quantum Dots. *J. Phys. Chem. C* **2007**, *111*, 5904.

DOI: 10.1021/acs.nanolett.9b03342
Nano Lett. 2019, 19, 8125−8131